Chemosphere 284 (2021) 131358

Contents lists available at ScienceDirect

Chemosphere

journal homepage: www.elsevier.com/locate/chemosphere

Integration of a nitrification bioreactor and an anoxic biotrickling filter for simultaneous ammonium-rich water treatment and biogas desulfurization

Patricio I. Cano, Fernando Almenglo, Martín Ramírez *, Domingo Cantero

Department of Chemical Engineering and Food Technology, Vine and Agri-Food Research Institute (IVAGRO), University of Cadiz, Pol. Río San Pedro s/n, Puerto Real, 11510, Spain

ARTICLE INFO

Handling editor: Derek Muir

Keywords:
Biological desulfurization
Anoxic conditions
Nitrification
Nitrogen removal optimization
Biogas
Nitrate equivalent

ABSTRACT

A preliminary assessment has been carried out on the integration of an anoxic biotrickling filter and a nitrification bioreactor for the simultaneous treatment of ammonium-rich water and H_2S contained in a biogas stream. The nutrient consumption in the biotrickling filter was as follows (mol^{-1} NO_3^--N): $6.3{\cdot}10^{-4} \pm 1.2{\cdot}10^{-4}$ mol PO_4^{3-}-P, 0.04 ± 0.05 mol NH_4^+-N and 0.04 ± 0.03 mol K^+-K. Furthermore, it was possible to supply a mixture of biogenic NO_3^- and NO_2^- into the biotrickling filter from the nitrification bioreactor to obtain a maximum elimination capacity of 152 gH_2S–S m^{-3} h^{-1}. The equivalence between the two compounds was 1 mol NO_3^--N equal to 1.6 mol NO_2^--N. The biotrickling filter was also operated under a stepped variable inlet load (30–100 gH_2S–S m^{-3} h^{-1}) and outlet H_2S concentrations of less than 150 ppm_V were obtained. It was also possible to maintain the outlet H_2S concentration close to 15 ppm_V with a feedback controller by manipulating the feed flow (in the nitrification bioreactor). Two stepped variable inlet loads were tested (60–111 and 16–102 gH_2S–S m^{-3} h^{-1}) under this type of control. The implementation of feedback control could enable the exploitation of biogas in a fuel cell, since the H_2S concentrations were 15.1 ± 4.3 and 15.0 ± 3.4 ppm_V. Finally, the anoxic biotrickling filter experienced partial denitrification and this implied a loss of the desulfurization effectiveness related to SO_4^{2-} production.

1. Introduction

Biotrickling filters (BTFs) have proven to be efficient and viable for biogas desulfurization (Andriamanohiarisoamanana et al., 2020). The biological desulfurization can be carried out under aerobic or anoxic conditions. Aerobic desulfurization is a low-cost technology because O_2 is used as the electron acceptor. The main drawback of aerobic processes is the low solubility of O_2, which causes S^0 accumulation on the packed bed. However, the use of an external device such as jet-venturi and control of the trickling liquid velocity (TLV) enhances the O_2 mass transfer in aerobic BTFs (López et al., 2018). In any case, the air supply can lead to biogas dilution or, in the case of malfunction, an explosive atmosphere concentration can be reached. In contrast, anoxic desulfurization does not suffer from these operational issues and the main drawback is the need for a source of NO_3^- or NO_2^-. It has been shown that the best alternative is the use of NO_3^- or NO_2^- from an available nitrification bioreactor (Cano et al., 2018).

Nitrification is a two-step process in which NH_4^+ is initially oxidized to NO_2^- by ammonia-oxidizing bacteria (AOB) and the NO_2^- is then oxidized to NO_3^- by nitrite-oxidizing bacteria (NOB). AOB and NOB have different optimum operating conditions, so the nitrification process can be controlled to produce NO_3^-, NO_2^- or both (Pedrouso et al., 2017; Reino et al., 2017).

Anoxic desulfurization is also a two-step process. The H_2S is oxidized to S^0 and then to SO_4^{2-}. In this case, the product selectivity depends on the nitrogen (NO_3^--N or NO_2^--N)–H_2S–S (N/S) ratio (Cano et al., 2019; Mora et al., 2015; Soreanu et al., 2008). In previous studies (Almenglo et al., 2016; Brito et al., 2019; Cano et al., 2019) the use of NO_3^- or NO_2^- has been successful regardless of the type of electron acceptor added to the medium. The amount of NO_2^--N required to desulfurize 1 mol of H_2S–S is higher than the one required for NO_3^--N, since the higher oxidizing power of the latter one. Therefore, in order to normalize the electron acceptor supply to the desulfurization bioreactor, González-Cortés et al. (2021) have introduced the NO_3^- equivalent ($[NO_3^-]_{eq}$) term. This NO_3^- equivalent is calculated as the sum of the concentration of NO_3^- and the concentration of NO_2^- corrected with an adjustment factor to take into consideration its lower oxidizing power. The determination of the $[NO_3^-]_{eq}$ is expressed by Equation (1), where

* Corresponding author.
E-mail address: martin.ramirez@uca.es (M. Ramírez).

https://doi.org/10.1016/j.chemosphere.2021.131358
Received 23 November 2020; Received in revised form 16 June 2021; Accepted 26 June 2021
Available online 2 July 2021

'a' is the adjustment factor:

$$[NO_3^-]_{eq} = [NO_3^-] + \frac{[NO_2^-]}{a} \quad (1)$$

Autotrophic denitrification using HS^- to remove NO_3^- or NO_2^- has been extensively described in the literature for wastewater treatment (Fajardo et al., 2012). However, the number of studies concerning the use of nitrified effluents for biogas desulfurization is limited (Deng et al., 2009; González-Cortés et al., 2021; Guerrero et al., 2020; Pirolli et al., 2016; Tanikawa et al., 2018; Wang et al., 2009; Xu et al., 2020; Zeng et al., 2019). As an example, González-Cortés et al. (2021) suggested a two-stage process for the commercialization of S^0. Guerrero et al. (2020) compared two different ways of carrying out the nitrification process coupled to a denitrification-desulfurization reactor, i.e., in the same reactor and in two different reactors. The systems employed were a bench scale aerobic horizontal fixed-bed reactor coupled with an anoxic vertical fixed-bed reactor (AHFBR-AVFBR) and a bench scale mixed aerobic-anoxic horizontal fixed-bed reactor (MAAFBR).

In the study described here, a continuous stirrer tank reactor (CSTR) with biomass recirculation and a BTF were used for the oxidation of NH_4^+ to NO_3^- and/or NO_2^- and subsequent autotrophic denitrification and HS^- oxidation, respectively. The bioreactors were operated using a continuous feed of ammonium-rich synthetic effluent to the CSTR, with the nitrified effluent subsequently fed to the BTF. The effect of an effluent nitrified with NO_3^- and NO_2^- on the H_2S removal efficiency (RE) was determined. Moreover, the operation of the system had feedback control to keep the outlet H_2S concentration constant and this was achieved by manipulation of the NH_4^+ feed to the CSTR. In addition, the effect of a NPK (nitrogen/phosphorus/potassium) fertilizer as a nutrient source was evaluated. Finally, it was tested where should be applied this NPK fertilizer (BTF or CSTR).

2. Materials and methods

2.1. Experimental setup

A schematic diagram of the BTF and CSTR is shown in Fig. 1. It can be seen that the BTF was fed with the nitrified effluent from the settler (number 19, Fig. 1) of the nitrification system. The pump P5 (Fig. 1) provided the same flow rate to feed the nitrification bioreactor (ammonium-rich source) and to feed the BTF. The flow rate could be controlled manually (open-loop) or by using control loop (supplementary Figure S1), which uses as the control variable the outlet H_2S concentration (number 13, Fig. 1) and as the manipulated variable the liquid flow rate of pump P5 (Fig. 1).

The anoxic BTF was made of transparent polyvinyl chloride (PVC)

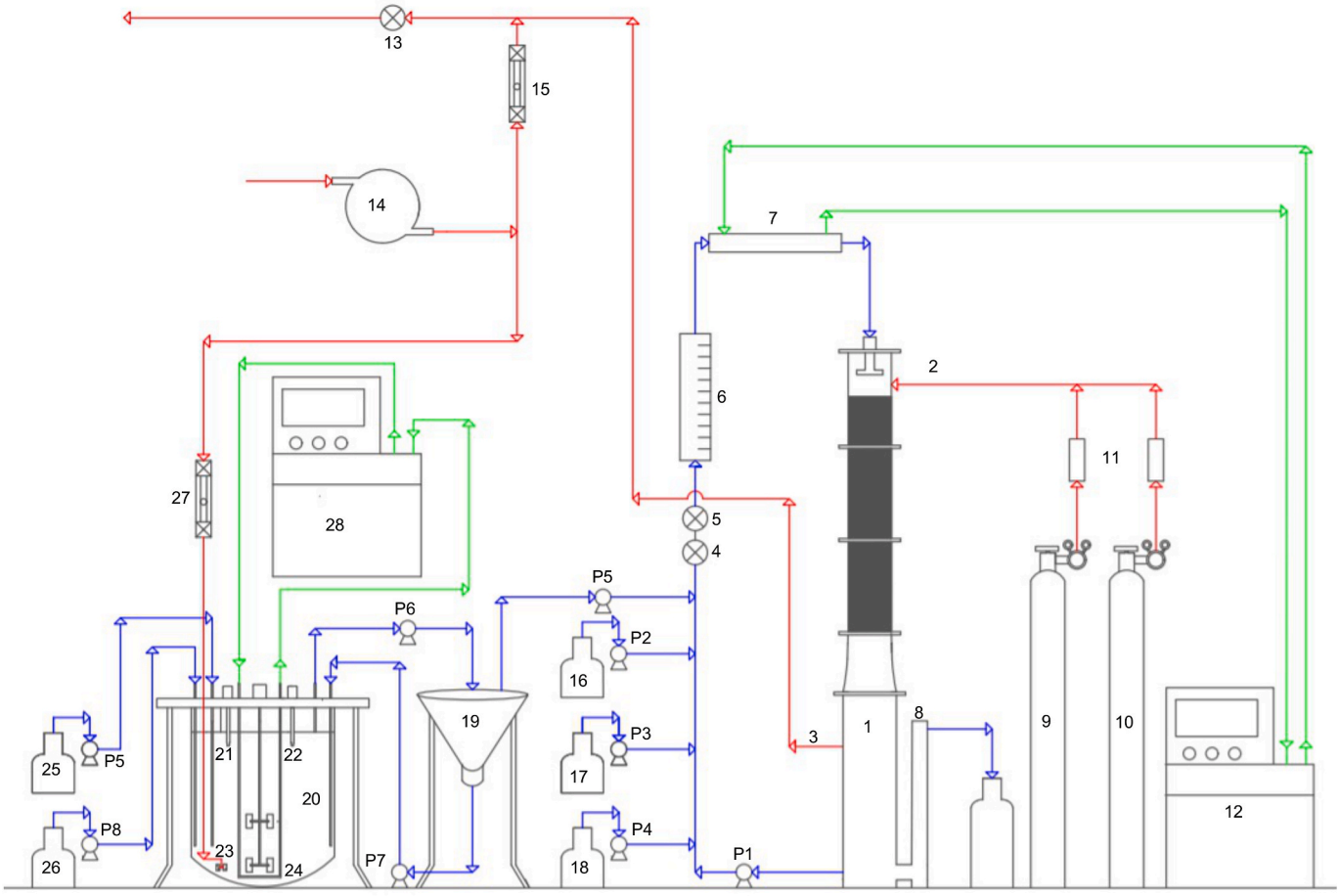

Fig. 1. Experimental setup. (1) Anoxic BTF, (2) Inlet gas (BTF), (3) Outlet gas (BTF), (4) ORP probe, (5) pH probe (BTF), (6) Liquid flow meter, (7) Heat exchanger (BTF), (8) Liquid purge (BTF), (9) N_2 cylinder, (10) H_2S cylinder, (11) Mass flow controller (BTF), (12) Thermostatic bath (BTF), (13) H_2S sensor for the control loop, (14) Compressed air stream, (15) Air flow meter for the proper performance of the H_2S sensor, (16) Mineral medium dosing tank (BTF), (17) Base dosing tank (BTF), (18) Acid dosing tank (BTF), (19) Settler, (20) Nitrification bioreactor, (21) pH probe (nitrification bioreactor), (22) DO probe, (23) Air Diffuser, (24) Heat exchanger (nitrification bioreactor), (25) NH_4^+ rich water tank (nitrification bioreactor), (26) $NaHCO_3$ tank (nitrification bioreactor), (27) Air flowmeter (nitrification bioreactor), (28) Thermostatic bath (nitrification bioreactor), (P1) Recirculation pump (BTF), (P2) Mineral medium dosing pump (BTF), (P3) Base dosing pump (BTF), (P4) Acid dosing pump (BTF), (P5) Variable speed pump controlled by voltage (BTF and nitrification bioreactor), (P6) Purging pump (nitrification bioreactor), (P7) Biomass recirculation pump (nitrification bioreactor), (P8) Base dosing pump (nitrification bioreactor).

(internal diameter 71.4 mm) and the packed bed was divided into three sections, with a total bed height of 500 mm: 200, 200 and 100 mm. The packing material was polypropylene Pall rings 5/8" (Pall Ring Company, UK) and the total bed volume and the volume of medium under recirculation were 2.1 and 3.7 L, respectively. A digital Multimeter 44 (Hach Lange Spain, S.L.U, Spain) was used for oxide-reduction potential (ORP) monitoring and pH was controlled (7.3–7.5) by the addition of NaOH (1 M) or H_3PO_4 (0.33 M). The temperature of the BTF was kept at 30 °C using a thermostatic bath (number 12, Fig. 1) and a heat exchanger (number 7, Fig. 1) in the inlet stream of the medium to the BTF.

The BTF was fed with substitute biogas (mixture of H_2S and N_2). The gas was supplied from two compressed gas cylinders (numbers 9 and 10, Fig. 1): N_2 (quality 99.9%) and mixture (50% H_2S, balance N_2) by means of mass flow controllers (Bronkhorst F–201C). The empty bed residence time (EBRT) was constant at 158 s and the substitute biogas was fed in co-current flow mode with a TLV of 10 m h^{-1}. These operational conditions were previously optimized by the authors (Cano et al., 2019).

An autoclavable glass bioreactor (Applikon Biotechnology, B.V., Netherlands) was used as the CSTR (number 20, Fig. 1). The total and working volumes were 7 and 5 L, respectively. Air was fed into the bioreactor at 0.1 vvm (vessel volume per minute) and the stirring speed was 200 rpm (revolution per minute). The pH was controlled at 7.3 (days 0–111) and 7.8 (days 112–354) by the addition of $NaHCO_3$ (0.6 M) in conjunction with a pH controller (AX466, ABB, S.A., Spain) and a pH electrode (TB551, ABB, S.A., Spain). The dissolved oxygen (DO) was measured periodically using a multimeter (6603, Mettler Toledo, LCC, Switzerland) equipped with an InPro 6050 probe. The temperature was controlled by a thermostatic bath (number 28, Fig. 1) using an internal coil (Fig. 1) at 20 or 30 °C (Table 1b). The outlet liquid stream was pumped (P6, Fig. 1) to a settler with a volume of 6 L. The clarified liquid from the settler was introduced into the BTF and the concentrated solid stream was returned to the CSTR by a peristaltic pump (P7, Fig. 1).

The whole system was controlled and monitored using a cDAQ chassis (NI-9184) equipped with three modules; current input (NI-9264), digital I/O module (NI-9375) and voltage output module (N-9264), with control achieved with LabVIEW™ 2015 (National Instruments Corp., USA).

2.2. Experimental conditions

The experimental conditions for the BTF and the CSTR are provided in Table 1a and 1b, respectively. Different mineral media were used in the two bioreactors. In the BTF, during the first 185 days of operation a dilute solution (1:400) prepared from NPK (6-4-6) fertilizer (Biovert, Manvert, Spain) at 306 mL h^{-1} was employed. The nutrient dosage was carried out in the nitrification bioreactor from day 185 to day 354. The NPK fertilizer composition was (g L^{-1}): K^+-K (26.9), SO_4^{2-}-S (4.6), PO_4^{3-}-P (7.8), NH_4^+-N (20.7), NO_2^--N (2.8) and NO_3^--N (20.2). In addition to the mineral medium, $NaHCO_3$ solution (50 mg L^{-1}) was provided as a carbon source. In the nitrification bioreactor a synthetic eluent (ammonium-rich water) was used. The nitrogen concentration was in the range 600–800 mg NH_4^+-N L^{-1} and its composition (Jubany et al., 2005) was (mg L^{-1}): KH_2PO_4 (20.0), NaCl (16.0), $MgCl_2{\cdot}7H_2O$ (18.0), $FeSO_4{\cdot}7H_2O$ (0.4), $MnSO_4{\cdot}H_2O$ (0.3), $ZnSO_4{\cdot}7H_2O$ (0.4), $CuSO_4{\cdot}5H_2O$ (0.2), H_3BO_3 ($2.0{\cdot}10^{-2}$) and $CaCl_2{\cdot}H_2O$ (8.0). From day 198, the mineral medium was replaced by dilute solutions of the NPK fertilizer from 1:40 to 1:200.

Table 1a
Experimental conditions (BTF).

Exp.	Days	Time (days)	Mineral Medium	HRT (h)	IL (gS-H_2S m^{-3} h^{-1})	$[H_2S]_{in}$
1	0–43	43	NPK	8.0	78.1	2620
2	44–139	96	Fertilizer		23.7–156.2	796–5210
3	140–163	14			30.0–100.0	1040–3350
		10		9.0		
4	164–197	22		Variable	60.0–111.0	1980–3720
		12	None[a]		16.0–102.0	500–3400
5	198–354	65		26.7	0–142.0	0–4740
		23		35.5	16.0–102.0	500–3400
		69		32.6		

[a] The mineral medium was dosed in the CSTR.

In experiment 1 the BTF performance was analyzed on using NPK fertilizer as a replacement for the conventional mineral medium reported by Cano et al. (2019). The nitrification bioreactor was fed with ammonium-rich water (805.7 ± 37.5 mg NH_4^+-N L^{-1}).

In experiment 2 changes were made to the nitrification bioreactor to enhance the partial nitrification of NH_4^+ to NO_2^-. In this experiment four periods were identified (Table 1b). In the first period, the temperature was increased up to 30 °C. This value is optimum to achieve a higher growth of AOB in comparison to NOB (Pedrouso et al., 2017). In the second period (discontinuous mode, Table 1), the nitrified effluent was stored in a tank with the aim of allowing modifications to the feed N:S ratio in the BTF. In the third period, the CSTR was operated in continuous mode and, finally, in the fourth period the pH was increased from 7.3 to 7.8 with the aim of reducing the free nitrous acid (FNA) concentration and increasing the free ammonia (FA) (Jianlong and Ning, 2004). As far as the NH_4^+ fed in the CSTR is concerned, the NH_4^+ concentration and the NH_4^+ load in the continuous and discontinuous periods were 816.2 ± 120.8 mg NH_4^+-N L^{-1} and 375–425 g NH_4^+-N m^{-3} d^{-1}, respectively.

The H_2S concentration value in a biogas plant is not constant throughout the day (Tomàs et al., 2009). Therefore, experiment 3 concerned an analysis of the BTF response under a stepped variable H_2S Inlet Load (IL) according to Equation (2) (sinusoidal profile) under open-loop conditions. The Equation (2) has been studied in previous studies (Brito et al., 2017, 2018; López et al., 2016), where '$[H_2S]$' and "t" are respectively the H_2S concentration (ppm_V) and time (hours). Two different cases were assessed: hydraulic residence times (HRT) of 32 and 8 h for the CSTR and BTF (Case 1) and HRT of 48 and 9 h for the CSTR and BTF (Case 2). The NH_4^+ concentration was between 600 and 800 mg NH_4^+-N L^{-1}.

$$[H_2S] = 1170 \cdot \sin\left(\frac{2\Pi}{24} \cdot t\right) + 2181 \quad (2)$$

In Experiment 4, two tests were carried out using feedback control based on the previous removal results obtained in experiment 3, since this experiment was useful to identify the removal limits in the BTF. In both tests the controlled parameter was the outlet H_2S concentration and the manipulated parameter was the flow rate of ammonium-rich water (concentration of 600–800 mg NH_4^+-N L^{-1}). The NPK fertilizer was fed into the anoxic BTF in the first trial (dilution of 1:400 and flow of 306 mL h^{-1}). NPK fertilizer was also fed into the nitrification bioreactor in the second trial by an additional peristaltic pump (dilution 1:40 and flow of 38 mL h^{-1}). Finally, the IL were modified using two sinusoidal equations (60–111 and 16–102 gH_2S–S m^{-3} h^{-1}), i.e., Equations (3) and (4) for the first and second test, respectively. The modification of the IL using Equation (4) allowed to test the effect of a lower H_2S inlet concentration (up to 500 ppm_V), whereas using Equation (3) the minimum H_2S concentration was (1890 ppm_V) (Table 1a).

$$[H_2S] = 860 \cdot \sin\left(\frac{2\Pi}{24} \cdot t\right) + 2840 \quad (3)$$

$$[H_2S] = 1430 \cdot \sin\left(\frac{2\Pi}{24} \cdot t\right) + 1980 \quad (4)$$

Experiment 5 involved a study of the effect of NPK fertilizer dosage in the nitrification bioreactor. Experiment 5 consisted of three distinct periods (Table 1b). In the first period, the NPK fertilizer was fed into the CSTR using an additional peristaltic pump (dilution of 1:40 and flow of 38 mL h^{-1}). In the second and third periods, the NPK fertilizer was added with the ammonium-rich water (dilutions of 1:40 and 1:200 in the

Table 1b
Experimental conditions (CSTR).

Exp.	Days	Duration (days)	Mineral Medium	HRT (h)	T (°C)	pH	Operation Mode
1	0–43	43	Mineral medium	32.0	20.0	7.3	Continuous
2	44–139	28			30.0		
		18					Discontinuous
		22					Continuous
		28				7.8	
3	140–163	14					
		10		48.0			
4	164–197	34		Variable			
5	198–354	65	NPK fertilizer	28.2	20.0		
		23		48.0			
		69		44.1			

second and third periods, respectively). The IL in the anoxic BTF was varied manually in the range 0–142 gH_2S–S m^{-3} h^{-1} according to supplementary Figure S2 in the first period. In the second and third periods (Table 1b) the H_2S IL was varied according to Equation (4).

2.3. NO_3^- equivalent

According to Soreanu et al. (2008) and Mahmood et al. (2007), the partial HS^- oxidation is described by the following equations:

$$5H_2S + 2NO_3^- \rightarrow 5S^0 + N_2 + 4H_2O + 2OH^- \quad (5)$$

$$3HS^- + 2NO_2^- + 5H^+ \rightarrow 3S^0 + N_2 + 4H_2O \quad (6)$$

$$5H_2S + 8NO_3^- \rightarrow 5SO_4^{2-} + 4N_2 + 4H_2O + 2H^+ \quad (7)$$

$$3HS^- + 8NO_2^- + 5H^+ \rightarrow 3SO_4^{2-} + 4N_2 + 4H_2O \quad (8)$$

Therefore, the N:S molar ratios needed to obtain a SO_4^{2-} production of 100% are 1.6 and 2.67 mol mol^{-1}, using NO_3^- and NO_2^-, respectively. Otherwise, 0.4 and 0.67 mol mol^{-1} are needed if 100% oxidation to S^0 is desired. Equations (5)–(8) are considered as kinetic 1.

Mora et al. (2015) consider a more complex stoichiometry, including biomass production and carbon and nitrogen assimilation (Eqs. (9)–(12)):

$$HS^- + 0.350\,NO_3^- + 1.40\,H^+ + 0.059\,HCO_3^- + 0.004\,CO_2 + 0.013\,NH_4^+ \rightarrow 0.013\,C_5H_7O_2N + 1.21\,H_2O + 0.175\,N_2 + S^0 \quad (9)$$

$$HS^- + 1.23\,NO_3^- + 0.537\,H^+ + 0.438\,HCO_3^- + 0.027\,CO_2 + 0.093\,NH_4^+ \rightarrow 0.093\,C_5H_7O_2N + 0.866\,H_2O + 0.614\,N_2 + SO_4^{2-} \quad (10)$$

$$HS^- + 0.587\,NO_2^- + 1.63\,H^+ + 0.057\,HCO_3^- + 0.004\,CO_2 + 0.012\,NH_4^+ \rightarrow 0.012\,C_5H_7O_2N + 1.326\,H_2O + 0.293\,N_2 + S^0 \quad (11)$$

$$HS^- + 2.36\,NO_3^- + 1.53\,H^+ + 0.215\,HCO_3^- + 0.013\,CO_2 + 0.046\,NH_4^+ \rightarrow 0.046\,C_5H_7O_2N + 1.30\,H_2O + 1.18\,N_2 + SO_4^{2-} \quad (12)$$

Therefore, the N:S molar ratios for 100% of SO_4^{2-} production are 1.23 and 2.36 mol mol^{-1}, for NO_3^- and NO_2^-, respectively. Otherwise, 0.35 and 0.587 mol mol^{-1} are needed for 100% oxidation to S^0. Equations (9)–(12) are considered as kinetic 2.

The adjustment factor "a" of Equation (1) can be calculated by doing a linear regression between NO_3^- and NO_2^- concentration for both kinetics (supplementary Figure S3 and Figure S4). 1.67 and 1.91 mol NO_2^--N (mol NO_3^--N)$^{-1}$ can be predicted for kinetics 1 and 2, respectively.

In addition, the same BTF was previously operated using chemical NO_3^- to report complete production of S^0 and SO_4^{2-} (kinetic 3) under N:S ratios equal to 0.32 and 1.46 mol N–NO_3^- mol^- H_2S–S (Cano et al., 2019). This kinetic was adjusted by means of varying the "a" parameter in Equation (1) from 1.1 to 1.7 mol NO_2^--N (mol NO_3^--N)$^{-1}$ to find the one with the lowest error between the experimental SO_4^{2-} concentration and estimated SO_4^{2-} concentration. The estimated SO_4^{2-} concentration was obtained as follows (Fig. 2):

2.4. Analytical methods

The major cations and anions in the liquid phase were determined on an ion chromatograph (Metrohm, 930 Compact IC Flex, Switzerland) equipped with a conductometric detector (ASTM, 2017; ASTM, 2016).

The outlet H_2S concentration was measured by two different specific H_2S sensors. The H_2S samples were taken in discontinuous (GasBadge Pro Gas Detector, Industrial Scientific, USA) and in continuous (Euro-Gas Management Services Ltd, UK) mode in experiments 1 and 2 and 3 to 5, respectively.

3. Results and discussion

3.1. Effect of NPK fertilizer on the biotrickling filter

In experiment 1 the RE kept almost constant (in the range 97.0–99.8%) (supplementary Figure S5). Therefore, differences were not detected due to the type of mineral medium. In fact, the H_2S removal in this experiment (NPK fertilizer usage) was similar to that obtained in a previous study in which the same medium was used (Cano et al., 2019).

The feed N:S ratio was 1.6 ± 0.1 mol NO_3^--N mol^{-1} S–H_2S as a consequence of the nitrified liquid from the CSTR (around 1.3 mol NO_3^--N mol^{-1} S–H_2S) plus the additional dosage contribution from the NPK fertilizer (around 0.3 mol NO_3^--N mol^{-1} S–H_2S). The mean SO_4^{2-} production was 98.3 ± 3.4% (supplementary Figure S5) and it was only different (58.4%) on day 1 as a result of the NPK fertilizer dose acclimatization.

The CSTR had an average NH_4^+ removal rate of 433.5 ± 33.8 g NH_4^+-N m^{-3} d^{-1}. The main final product was NO_3^- (99.1 ± 0.1%) because NOB was not limited as a consequence of the optimal conditions employed, namely the low free HNO_2 concentrations ($1.7 \cdot 10^{-5}$ – $2.5 \cdot 10^{-4}$ mg HNO_2–N L^{-1}) and the fact that the system was operated at room temperature (Svehla et al., 2017).

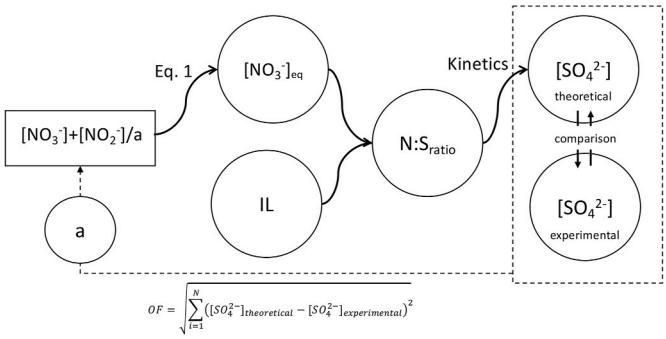

Fig. 2. Procedure for calculation of the adjustment factor "a".

Macro-element consumption is rarely reported in studies on anoxic biogas desulfurization. However, the importance of this parameter has been demonstrated (Almenglo et al., 2016; Moon et al., 2008). The PO_4^{3-}, K^+ and NH_4^+ consumption levels in the BTF were as follows (mol^{-1} NO_3^--N): $6.3{\cdot}10^{-4} \pm 1.2{\cdot}10^{-4}$ mol PO_4^{3-}-P, 0.04 ± 0.05 mol NH_4^+-N and 0.04 ± 0.03 mol K^+-K. Additionally, the maximum consumption levels were (mol^{-1} NO_3^--N): $7.35{\cdot}10^{-4}$ mol PO_4^{3-}-P, 0.18 mol NH_4^+-N and 0.10 mol K^+-K. As a consequence, the phosphorus uptake was negligible, although the effect of phosphorus on autotrophic denitrification has been reported (Fan et al., 2018; Moon et al., 2008). For instance, Moon et al. (2008) used a S^0-based column to evaluate the autotrophic denitrification of contaminated groundwater. It was found that NO_3^- removal did not occur during the first 60 days because PO_4^{3-} was not available. The system was later dosed with KH_2PO_4 and this enhanced the NO_3^- removal. Furthermore, it has been reported that there is a group of sulfur-oxidizing bacteria (large sulfur bacteria) that uptakes phosphorus by accumulation as polyphosphate (Lin et al., 2018). The ions NH_4^+ and K^+ showed the highest consumption rates. K^+ is the major intracellular cation in bacteria and it can play four roles: (i) an osmotic solute, (ii) a regulator of internal pH, (iii) an activator of intracellular enzymes and (iv) a second messenger (Epstein, 2003). Nitrogen from NH_4^+ is an important source of nitrogen for bacteria, since most bacteria can assimilate this cation. NO_3^- is also efficiently assimilated but not as well as NH_4^+. In this sense, 15% of the weight of dry cells is nitrogen because of the presence of high levels in proteins and nucleic acids (Morgenroth et al., 1996). The unstable consumption of NH_4^+ could be due to the use of NH_4^+ and NO_3^- as the nitrogen source. In fact, different anoxic desulfurization kinetics have been reported for biomass growth on using both NO_3^- and NH_4^+ as the nitrogen source (Mora et al., 2015; Munz et al., 2015). For instance, Mora et al. (2015) described the anoxic desulfurization kinetics with cellular growth and they found NH_4^+ assimilation of 0.0756 mol NH_4^+-N mol^{-1} N–NO_3^- (anoxic) for complete oxidation to SO_4^{2-}. Furthermore, it has been reported that $(NH_4)_2SO_4$ was deposited on the packing of one biofilter that was used to assess the simultaneous removal of H_2S and NH_3 (Kim et al., 2002).

The K^+ ion has been studied previously, but only under heterotrophic conditions (Wang et al., 2020), where the denitrification rate increased 1.15–1.88-fold. In this sense, they found an increase in the diversity and abundance of microorganisms for concentrations below 229.78 ± 25.8 mg K^+-K L^{-1}, since this value involved biomass inhibition. They also found that the genera *Pseudomonas* (1.86%) and *Thiobacillus* (1.52%) only showed functional species for a K^+ concentration near 150 mg K^+-K L^{-1}. This value exhibited the highest NO_3^- removal. Moreover, the high variability of K^+ uptake could be due to the generation of solid deposits (Filho et al., 2010). In any case, this solid formation is probably not significant compared to the S^0 formation, because anoxic BTFs have been operated using KNO_3 without operational problems due to solid accumulation (Fernández et al., 2014).

3.2. Nitrification bioreactor performance: partial nitrification

During operation of the CSTR in experiment 2 the NO_2^- concentrations were kept high during the continuous operations (days: 44–71 and 89–139). The average values of the volumetric uptake during these periods were 392.0 ± 78.7 and 455.0 ± 80.2 g NH_4^+-N m^{-3} d^{-1}, respectively.

The average free HNO_2 concentration in this period was 0.04 ± 0.01 mg HNO_2–N L^{-1}. A similar value has been reported to suppress growth of NOB (Pedrouso et al., 2017). The pH during the second continuous period was changed on day 111 from 7.3 to 7.8 and this had a significant influence on the HNO_2 concentration (supplementary Figure S6). This change coincided with a slight increase in the NO_3^- concentration in the CSTR (from 104.6 to 150 mg NO_3^--N L^{-1}). Therefore, the lower HNO_2 concentration could cause NOB proliferation (Pedrouso et al., 2017).

3.3. Effect of a combined NO_3^- and NO_2^- feed in the anoxic BTF

In experiment 2 the IL for the BTF varied in the range 23.7–156.2 gH_2S–S m^{-3} h^{-1} (supplementary Figure S7) during the 96 days of operation. The RE oscillated in the range 92.4–100%. Hence, a limitation was not found in the BTF for the use of biogenic NO_2^-/NO_3^-. The coupling of a CSTR to an anoxic BTF for nitrification and desulfurization is therefore a promising approach that is worth pursuing.

The critical and maximum elimination capacities (EC_{CRIT} and the EC_{MAX}) were 119.5 (RE of 99.1%) and 151.9 (RE of 97.3%) gH_2S–S m^{-3} h^{-1}, respectively (Fig. 3).

To our knowledge, the EC_{MAX} obtained in the current work is the highest value reported for an anoxic desulfurization bioreactor in which biogenic NO_3^- and NO_2^- have been used (Deng et al., 2009; Lu et al., 2012; Wang et al., 2009; Zeng et al., 2019). For instance, González-Cortés et al. (2021) (blue squares in Fig. 3) tested the coupling of a CSTR for landfill leachate nitrification and a gas-lift reactor to desulfurize substitute biogas while promoting S^0 production at laboratory scale, with an EC_{MAX} of 141.2 gH_2S–S m^{-3} h^{-1} reported.

The results reported here are comparable to those obtained in studies carried out under commercial NO_2^- and NO_3^- feeds. For instance, the ECs obtained by Fernández et al. (2013), Almenglo et al. (2016),

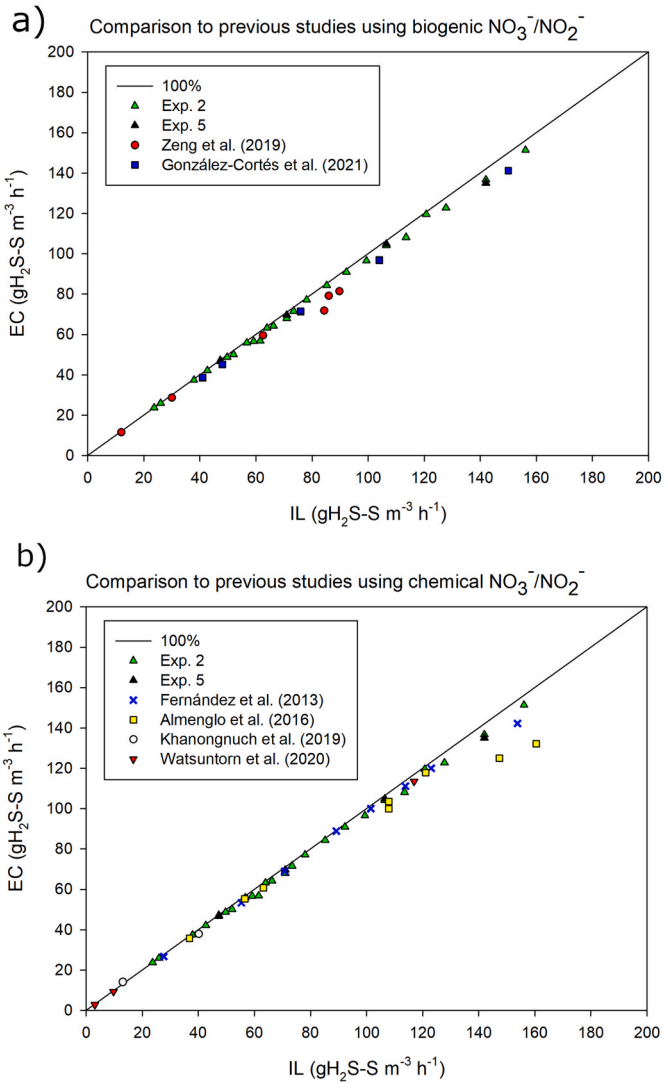

Fig. 3. EC versus IL under biological NO_3^- and NO_2^- feeds in Experiments 2 and 5 along with comparative data from studies by other authors using biogenic NO_2^-/NO_3^- (subfigure 3a) and chemical NO_2^-/NO_3^- (subfigure 3b).

Khanongnuch et al. (2019) and Watsuntorn et al. (2020) are shown in Fig. 3b.

3.4. NO_3^- equivalent ratio

For kinetics 1 and 2, the value of term "a" in equation (1) was of 1.67 and 1.91 mol NO_2^--N (mol NO_3^--N)$^{-1}$, respectively (supplementary Figure S3 and Figure S4). However, Kinetic 3 had an equivalence of 1.6 mol NO_2^--N equal to 1 mol $NO_{3\,eq}^-$-N (supplementary Figure S8). Therefore, the adjustment value was similar to the kinetic 1.

The removal of NO_2^- and NO_3^- in the BTF is represented in Fig. 4. Almost complete removal of both species was achieved during the first 20 days of this experiment (days 43–63) because there had been previous accumulation of S^0. The N:S ratios in this time period were very high (1.5–4.3 mol $NO_{3\,eq}^-$-N mol^{-1} H_2S–S).

The accumulation of NO_2^- took place later (from day 63–89) in the BTF because the N:S ratios remained very high and the accumulated S^0 had already been oxidized. In this context, better removal of NO_3^- was achieved because the anoxic BTF had been using NO_3^- as an electron acceptor up to this point (500 days of operation) (Cano et al., 2019). Nevertheless, other authors have found that NO_2^- is removed more efficiently than NO_3^- (Moraes et al., 2012; Zeng et al., 2019).

3.5. Integrated system performance under a stepped variable IL feed (open-loop conditions)

The CSTR and BTF were operated under a stepped variable H_2S IL (sinusoidal profile) in the BTF in experiment 3 in order to study the H_2S RE. Two different conditions were assessed, namely Case 1 (HRT in the CSTR and BTF of 32 and 8 h, respectively) and Case 2 (HRT in the CSTR and BTF of 48 and 9 h, respectively). The NO_2^- contribution was important in Case 1 (Fig. 5a) (the NO_3^- equivalent ratio was determined to be 1.6 mol NO_2^--N equal to 1 mol NO_3^--N, based on kinetic 3). In this context, the average values of the NH_4^+ volumetric uptake in Case 1 were 434.0 ± 20.1 g NH_4^+-N m^{-3} d^{-1}. It was promoted NO_2^- over NO_3^- production. As a matter of fact, the concentrations were 323.3 ± 15.2 mg NO_2^--N L^{-1} and 246.2 mg NO_3^--N L^{-1}, respectively. In contrast, the NO_2^- contribution was practically null in Case 2 because the CSTR was producing mainly NO_3^- during this period as a consequence of the excessive HRT (48 h) in the CSTR and the low levels of HNO_2 present ($8.5{\cdot}10^{-6}$–0.01 mg HNO_2–N L^{-1}) (Fig. 5b). In fact, the NO_2^- and NO_3^- concentrations were equal to 130.6 ± 77.9 mg NO_2^--N L^{-1} and 460.9 ± 82.6 mg NO_3^--N L^{-1} (NH_4^+ volumetric uptake equal to 295.1 ± 28.6 g NH_4^+-N m^{-3} d^{-1}). Nevertheless, RE were similar, since the N:S ratios did not differ much (Fig. 5).

3.6. Utilization of a feedback controller to maintain the H_2S concentration below 20 ppm_V

The feedback control was type PI based on preliminary tests performed on the integrated system (CSTR coupled to the BTF) to avoid a delay effect. Consequently, the 2 parameter tunings that characterize PI controllers, proportional gain (K_p) and integral gain (K_i), were found according to the method reported by Astrom and Hägglund (1995). Hence these values were 0.02025 (K_p) and $5.19231{\cdot}10^{-5}$ (K_i).

Experiment 4 involved the implementation of a feedback controller under two stepped variable IL (sinusoidal profiles): the first one was 60–111 gH_2S–S m^{-3} h^{-1} and the second one was 16–102 gH_2S–S m^{-3} h^{-1}.

The feedback controller was capable of maintaining the H_2S concentration close to 15 ppm_V (15.1 ± 4.3 ppm_V) in the IL range 60–111 gH_2S–S m^{-3} h^{-1}, as shown in Fig. 6a.

The test with the IL profile in the range 16–102 gH_2S–S m^{-3} h^{-1} also gave a concentration in the outlet that was close to 15 ppm_V (15.0 ± 3.4 ppm_V), as shown in Fig. 6b.

The ORP values fluctuated significantly in this experiment. For instance, the minimum ORP value was −424 mV at 29.3 gH_2S–S m^{-3} h^{-1}. This very low ORP value was due to the NPK fertilizer fed into the CSTR, in contrast to the other trial performed in the current study with feedback control (under a stepped variable H_2S variation of 60–111 gH_2S–S m^{-3} h^{-1}). Low ORP values are undesirable because they can lead to H_2S accumulation in the liquid phase of the BTF.

Feedback control was applied in the current study to reach H_2S concentrations that would be suitable to valorize the desulfurized biogas in a fuel cell, i.e., type Phosphoric Acid Fuel Cell (PAFC) coupling two sequential continuous bioreactors (Awe et al., 2017).

3.7. Effect of the nutrient dosage into the nitrification bioreactor in the integrated system

The NPK fertilizer was dosed into the BTF in experiments 1–4. Finally, the dose point was changed to the CSTR in experiment 5 and this did not have any adverse effect on performance. In fact, the maximum NH_4^+ removal was 401.5 ± 72.7 g NH_4^+-N m^{-3} d^{-1}. The final oxidation product was NO_3^- in all periods (Table 1b, experiment 5).

The accumulation of NO_2^- was detected in the BTF for the first HRT of

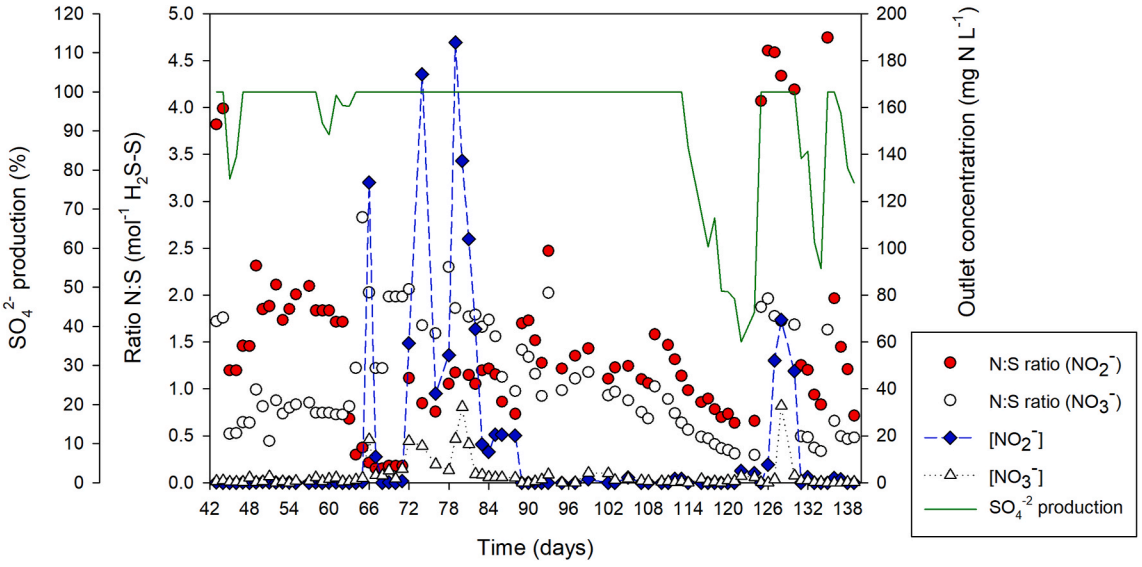

Fig. 4. N:S ratio (NO_2^- and NO_3^-), NO_2^- and NO_3^- concentrations and SO_4^{2-} production versus time (Experiment 2).

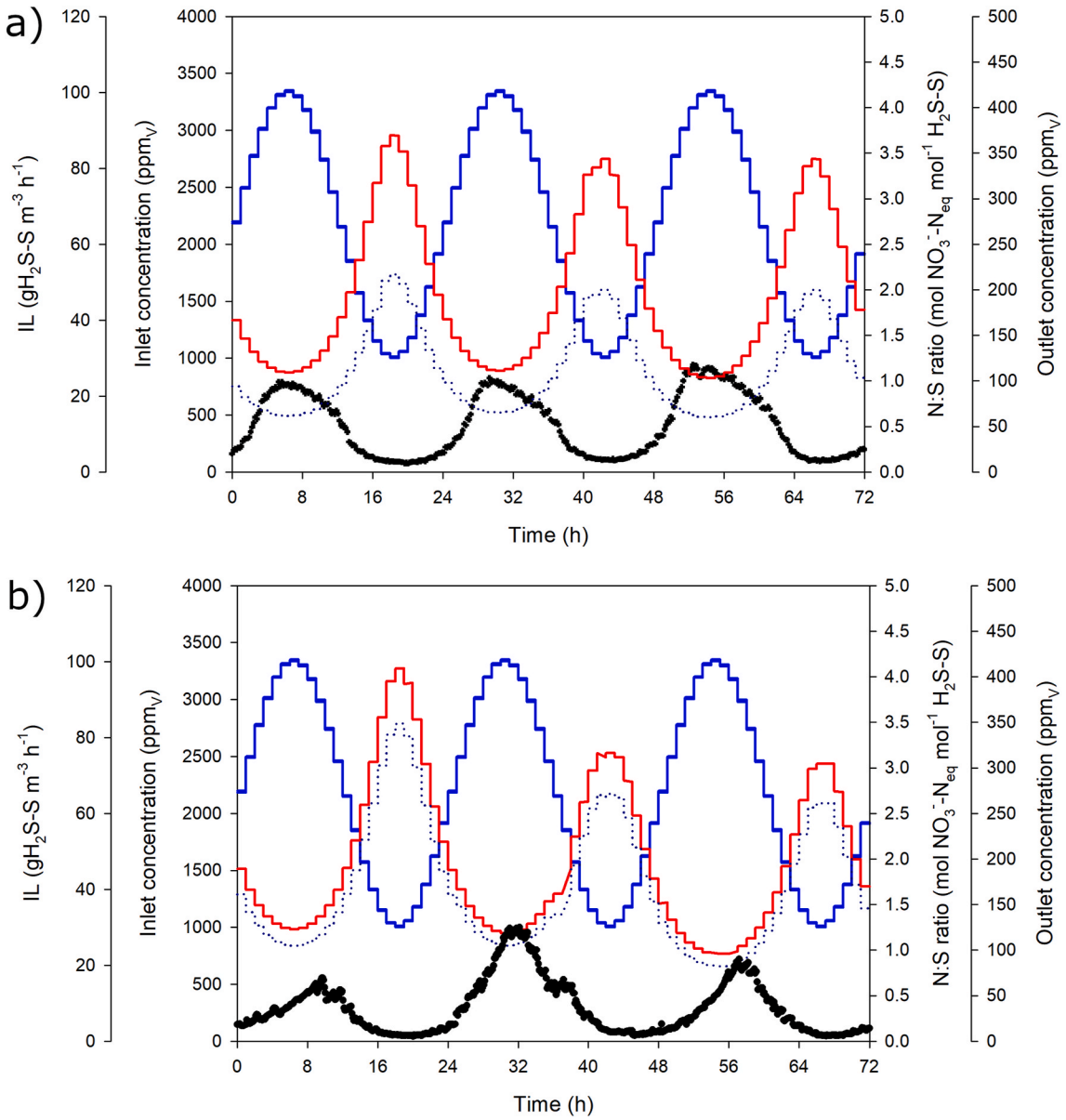

Fig. 5. H_2S concentration and N:S ratio for a stepped variable H_2S IL of 30–100 gS-H_2S m^{-3} h^{-1}. Legend: IL and inlet concentration (blue), N:S ratio considering $NO_{3\,eq}^-$ (red), N:S ratio considering NO_3^- and excluding NO_2^- (dotted line) and outlet concentration (black). (For interpretation of the references to colour in this figure legend, the reader is referred to the Web version of this article.)

26.7 h (Table 1a, experiment 5) as a result of partial denitrification in the bioreactor (days 198–263, Table 1). The partial denitrification did not lead to a decrease in H_2S removal and RE varied in the range 92.7–100% (Fig. 3). Nevertheless, the partial denitrification led to a decrease in the effectiveness due to SO_4^{2-} production, i.e., 36.6–94.4% for N:S feed ratios of 0.7–2.0 mol $NO_{3\,eq}^-$-N mol^{-1} H_2S–S. Therefore, the predicted SO_4^{2-} production rates according to the three kinetics discussed in section 3.3 were compared to the experimental SO_4^{2-} value. The best approach in this respect was again provided by kinetic 3 (supplementary Figure S9).

Chen et al. (2018) have suggested all existing NO_3^- should be reduced to NO_2^- before the NO_2^- reduction. In fact, the NO_2^- accumulation was associated with an excess of NO_3^- concentration. Therefore, the NO_3^- concentration must be as low as possible to promote the further NO_2^- reduction. Hence, NO_3^- and NO_2^- concentrations have to be controlled to avoid partial denitrification.

Other authors have previously detected NO_2^- accumulation as a result of partial autotrophic and heterotrophic denitrification in anoxic desulfurization (Oberoi et al., 2021; Pan et al., 2013). As far as autotrophic denitrification is concerned, Oberoi et al. (2021) found a significant influence of the supply of electrons by the reduced sulfur compound (H_2S or S^0) during their oxidation and the competition for electrons between all reductases involved in the nitrogen compound (NO_3^-, NO_2^-, NO and N_2O) reduction. This influence could be the cause of the NO_2^- accumulation in the case reported here.

4. Conclusions

The results of the current study prove the possibility of successfully coupling a nitrification bioreactor and an anoxic BTF for the simultaneous treatment of ammonium-rich water and H_2S contained in a biogas flow.

The BTF performance is not affected by the electron acceptor from the nitrification bioreactor, since biogenic NO_2^- and NO_3^- can be simultaneously supplied. In this sense, the equivalence between these two species is 1 mol NO_3^--N equal to 1.6 mol NO_2^--N. Moreover, the EC_{MAX}

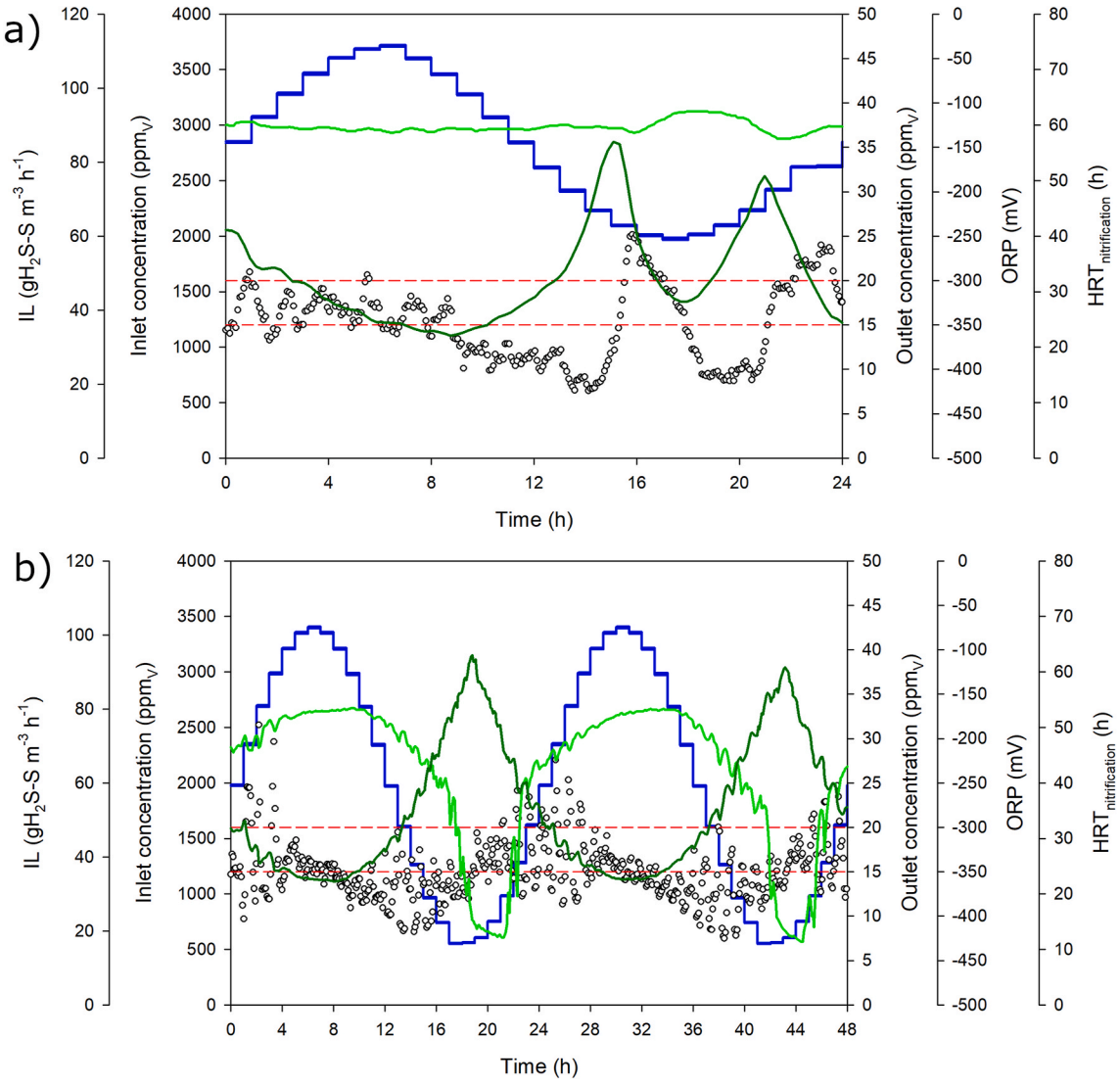

Fig. 6. H_2S concentration, ORP and HRT of the CSTR in Experiment 4. Legend: IL and inlet concentration (blue), ORP (light green), HRT in the nitrification reactor (dark green), outlet concentration = 15 and 20 ppm_v (red lines) and outlet concentration (circles). (For interpretation of the references to colour in this figure legend, the reader is referred to the Web version of this article.)

obtained on using biogenic NO_2^-/NO_3^- was 152 gH_2S–S m^{-3} h^{-1}. In regard to the nutrient consumption in the BTF were (mol^{-1} NO_3^--N): $6.3{\cdot}10^{-4} \pm 1.2{\cdot}10^{-4}$ mol PO_4^{3-}-P, 0.04 ± 0.05 mol NH_4^+-N and 0.04 ± 0.03 mol K^+-K.

The H_2S concentration was maintained close to 15 ppm_V by means of a control strategy that involved manipulating the feed flow (in the nitrification bioreactor) based on the H_2S concentration in the outlet. Two IL were tested: 60–111 and 16–102 g H_2S–S m^{-3} h^{-1}. The use of this control strategy could enable subsequent biogas exploitation in a PAFC.

Finally, the anoxic BTF suffered from partial denitrification, which led to a decrease in the effectiveness of the desulfurization process due to SO_4^{2-} production drop.

Credit author statement

Patricio Iván Cano: Investigation, Formal analysis, Writing – original draft preparation. Fernando Almenglo: Conceptualization, Methodology, Writing- Reviewing and Editing. Martín Ramírez: Conceptualization, Methodology, Supervision, Project administration, Funding acquisition, Writing- Reviewing and Editing. Domingo Cantero: Conceptualization, Supervision, Project administration, Funding acquisition, Writing- Reviewing and Editing.

Declaration of competing interest

The authors declare that they have no known competing financial interests or personal relationships that could have appeared to influence the work reported in this paper.

Acknowledgments

The Spanish Government (Ministerio de Economía y Competitividad) and European FEDER funds provided financial support through the project CTM2012-37927-C03 'Monitoring, modelling and control towards the optimization of anoxic and aerobic desulfurizing biotrickling filters'.

Appendix A. Supplementary data

Supplementary data to this article can be found online at https://doi.org/10.1016/j.chemosphere.2021.131358.

References

Almenglo, F., Ramírez, M., Gómez, J.M., Cantero, D., 2016. Operational conditions for start-up and nitrate-feeding in an anoxic biotrickling filtration process at pilot scale. Chem. Eng. J. 285, 83–91. https://doi.org/10.1016/j.cej.2015.09.094.

Andriamanohiarisoamanana, F.J., Yasui, S., Iwasaki, M., Yamashiro, T., Ihara, I.K.U., 2020. Performance study of a bio-trickling filter to remove high hydrogen sulfide concentration from biogas: a pilot-scale experiment. J. Mater. Cycles Waste Manag. 22, 1390–1398. https://doi.org/10.1007/s10163-020-01031-4.

ASTM, 2017. D4327 Standard Test Method for Anions in Water by Suppressed Ion Chromatography, ASTM Inter. West Conshohocken, USA.

ASTM, 2016. D6504 Standard Practice for On-Line Determination of Cation Conductivity in High Purity Water. ASTM Inter, West Conshohocken, USA.

Astrom, K.J., Hägglund, T., 1995. PID Controllers: Theory, Design, and Tuning. Instrument Society of America, Research Triangle Park, NC, USA, ISBN 1556175167.

Awe, O.W., Zhao, Y., Nzihou, A., Minh, D.P., Lyczko, N., 2017. A review of biogas utilisation, purification and upgrading technologies. Waste Biomass Valorization 8, 267–283. https://doi.org/10.1007/s12649-016-9826-4.

Brito, J., Almenglo, F., Ramírez, M., Gómez, J.M., Cantero, D., 2017. PID control system for biogas desulfurization under anoxic conditions. J. Chem. Technol. Biotechnol. 92, 2369–2375. https://doi.org/10.1002/jctb.5243.

Brito, J., Valle, A., Almenglo, F., Ramírez, M., Cantero, D., 2018. Progressive change from nitrate to nitrite as the electron acceptor for the oxidation of H_2S under feedback control in an anoxic biotrickling filter. Biochem. Eng. J. 139, 154–161. https://doi.org/10.1016/j.bej.2018.08.017.

Brito, J., Almenglo, F., Ramírez, M., Cantero, D., 2019. Feedback and feedforward control of a biotrickling filter for H_2S desulfurization with nitrite as electron acceptor. Appl. Sci. 9, 2669. https://doi.org/10.3390/app9132669.

Cano, P.I., Brito, J., Almenglo, F., Ramírez, M., Gómez, J.M., Cantero, D., 2019. Influence of trickling liquid velocity, low molar ratio of nitrogen/sulfur and gas-liquid flow pattern in anoxic biotrickling filters for biogas desulfurization. Biochem. Eng. J. 148, 205–213. https://doi.org/10.1016/j.bej.2019.05.008.

Cano, P.I., Colón, J., Ramírez, M., Lafuente, J., Gabriel, D., Cantero, D., 2018. Life cycle assessment of different physical-chemical and biological technologies for biogas desulfurization in sewage treatment plants. J. Clean. Prod. 181, 663–674. https://doi.org/10.1016/j.jclepro.2018.02.018.

Chen, F., Li, X., Gu, C., Huang, Y., Yuan, Y., 2018. Selectivity control of nitrite and nitrate with the reaction of S^0 and achieved nitrite accumulation in the sulfur autotrophic denitrification process. Bioresour. Technol. 266, 211–219. https://doi.org/10.1016/j.biortech.2018.06.062.

Deng, L., Chen, H., Chen, Z., Liu, Y., Pu, X., Song, L., 2009. Process of simultaneous hydrogen sulfide removal from biogas and nitrogen removal from swine wastewater. Bioresour. Technol. 100, 5600–5608. https://doi.org/10.1016/j.biortech.2009.06.012.

Epstein, W., 2003. The roles and regulation of potassium in bacteria. In: Moldave, K. (Ed.), Progress in Nucleic Acid Research and Molecular Biology-, vol. 75. Academic Press, Massachusetts, USA, pp. 293–320. https://doi.org/10.1016/S0079-6603(03)75008-9.

Fajardo, C., Mosquera-Corral, A., Campos, J.L., Méndez, R., 2012. Autotrophic denitrification with sulphide in a sequencing batch reactor. J. Environ. Manag. 113, 552–556. https://doi.org/10.1016/j.jenvman.2012.03.018.

Fan, C., Wang, P., Zhou, W., Wu, S., He, S., Huang, J., Cao, L., 2018. The influence of phosphorus on the autotrophic and mixotrophic denitrification. Sci. Total Environ. 643, 127–133. https://doi.org/10.1016/j.scitotenv.2018.06.185.

Fernández, M., Ramírez, M., Gómez, J.M., Cantero, D., 2014. Biogas biodesulfurization in an anoxic biotrickling filter packed with open-pore polyurethane foam. J. Hazard Mater. 264, 529–535. https://doi.org/10.1016/j.jhazmat.2013.10.046.

Fernández, M., Ramírez, M., Pérez, R.M., Gómez, J.M., Cantero, D., 2013. Hydrogen sulphide removal from biogas by an anoxic biotrickling filter packed with Pall rings. Chem. Eng. J. 225, 456–463. https://doi.org/10.1016/j.cej.2013.04.020.

Filho, J.L.R.P., Sader, L.T., Damianovic, M.H.R.Z., Foresti, E., Silva, E.L., 2010. Performance evaluation of packing materials in the removal of hydrogen sulphide in gas-phase biofilters: polyurethane foam, sugarcane bagasse, and coconut fibre. Chem. Eng. J. 158, 441–450. https://doi.org/10.1016/j.cej.2010.01.014.

González-Cortés, J.J., Almenglo, F., Ramírez, M., Cantero, D., 2021. Simultaneous removal of ammonium from landfill leachate and hydrogen sulfide from biogas using a novel two-stage oxic-anoxic system. Sci. Total Environ. 750, 141664. https://doi.org/10.1016/j.scitotenv.2020.141664.

Guerrero, R.B.S., dos Santos, C.E.D., Soares, L.A., Zaiat, M., 2020. Comparison between two different fixed-bed reactor configurations for nitrogen removal coupled to biogas biodesulfurization. Biochem. Eng. J. 162, 107716. https://doi.org/10.1016/j.bej.2020.107716.

Jianlong, W., Ning, Y., 2004. Partial nitrification under limited dissolved oxygen conditions. Process Biochem. 39, 1223–1229. https://doi.org/10.1016/j.bej.2020.107716.

Jubany, I., Baeza, J.A., Carrera, J., Lafuente, F.J., 2005. Respirometric calibration and validation of a biological nitrite oxidation model incluiding biomass growth and substrate inhibition. Water Res. 39, 4574–4584. https://doi.org/10.1016/j.watres.2005.08.019.

Khanongnuch, R., Di Capua, F., Lakaniemi, A.-M., Rene, E.R., Lens, P.N.L., 2019. Transient-state operation of an anoxic biotrickling filter for H_2S removal. J. Hazard Mater. 377, 42–51. https://doi.org/10.1016/j.jhazmat.2019.05.043.

Kim, H., Kim, Y.J., Chung, J.S., Xie, Q., 2002. Long-term operation of a biofilter for simultaneous removal of H_2S and NH_3. J. Air Waste Manag. Assoc. 52, 1389–1398. https://doi.org/10.1080/10473289.2002.10470871.

Lin, S., Mackey, H.M., Hao, T., Guo, G., van Loosdrecht, M.C.M., Chen, G., 2018. Biological sulfur oxidation in wastewater treatment: a review of emerging opportunities. Water Res. 143, 399–415. https://doi.org/10.1016/j.watres.2018.06.051.

López, L.R., Dorado, A.D., Mora, M., Gamisans, X., Lafuente, J., Gabriel, D., 2016. Modeling an aerobic biotrickling filter for biogas desulfurization through a multi-step oxidation mechanism. Chem. Eng. J. 294, 447–457. https://doi.org/10.1016/j.cej.2016.03.013.

López, L.R., Brito, J., Mora, M., Almenglo, F., Baeza, J.A., Ramírez, M., Lafuente, J., Cantero, D., Gabriel, D., 2018. Feedforward control application in aerobic and anoxic biotrickling filters for H_2S removal from biogas. J. Chem. Technol. Biotechnol. 93, 2307–2315. https://doi.org/10.1002/jctb.5575.

Lu, H., Ekama, G.A., Wu, D., Feng, J., van Loosdrecht, M.C.M., Chen, G.H., 2012. SANI process realizes sustainable saline sewage treatment: steady state model-based evaluation of the pilot-scale trial of the process. Water Res. 46, 475–490. https://doi.org/10.1016/j.watres.2011.11.031.

Mahmood, Q., Zheng, P., Cai, J., Wu, D., Hu, B., Li, J., 2007. Anoxic sulfide biooxidation using nitrite as electron acceptor. J. Hazard Mater. 147, 249–256. https://doi.org/10.1016/J.JHAZMAT.2007.01.002.

Moon, H.S., Shin, D.Y., Kim, K.N.J.Y., 2008. A long-term performance test on an autotrophic denitrification column for application as a permeable reactive barrier. Chemosphere 73, 723–728. https://doi.org/10.1016/j.chemosphere.2008.06.065.

Mora, M., Fernández, M., Gómez, J.M., Cantero, D., Lafuente, J., Gamisans, X., Gabriel, D., 2015. Kinetic and stoichiometric characterization of anoxic sulfide oxidation by SO-NR mixed cultures from anoxic biotrickling filters. Appl. Microbiol. Biotechnol. 99, 77–87. https://doi.org/10.1007/s00253-014-5688-5.

Moraes, B.S., Souza, T.S.O., Foresti, E., 2012. Effect of sulfide concentration on autotrophic denitrification from nitrate and nitrite in vertical fixed-bed reactors. Process Biochem. 47, 1395–1401. https://doi.org/10.1016/j.procbio.2012.05.008.

Morgenroth, E., Schroeder, E.D., Chang, D.P.Y., Scow, K.M., 1996. Nutrient limitation in a compost biofilter degrading hexane. J. Air Waste Manag. Assoc. 46, 300–308. https://doi.org/10.1080/10473289.1996.10467464.

Munz, G., Mannucci, A., Arreola-Vargas, J., Alatriste-Mondragon, F., Giaccherini, F., Mori, G., 2015. Nitrite and nitrate as electron acceptors for biological sulphide oxidation. Water Sci. Technol. 72, 593–599. https://doi.org/10.2166/wst.2015.252.

Oberoi, A.S., Huang, H., Khanal, S.K., Sun, L., Lu, H., 2021. Electron distribution in sulfur-driven autotrophic denitrification under different electron donor and acceptor feeding schemes. Chem. Eng. J. 404, 126486. https://doi.org/10.1016/j.cej.2020.126486.

Pan, Y., Ye, L., Yuan, Z., 2013. Effect of H_2S on N_2O reduction and accumulation during denitrification by methanol utilizing denitrifiers. Environ. Sci. Technol. 47, 8408–8415. https://doi.org/10.1021/es401632r.

Pedrouso, A., Val del Río, A., Morales, N., Vázquez-Padín, J.R., Campos, J.L., Méndez, R., Mosquera-Corral, A., 2017. Nitrite oxidizing bacteria suppression based on in-situ free nitrous acid production at mainstream conditions. Separ. Purif. Technol. 186, 55–62. https://doi.org/10.1016/j.seppur.2017.05.043.

Pirolli, M., da Silva, M.L.B., Mezzari, M.P., Michelon, W., Prandini, J.M., Soares, H.M., 2016. Methane production from a field-scale biofilter designed for desulfurization of biogas stream. J. Environ. Manag. 177, 161–168. https://doi.org/10.1016/j.jenvman.2016.04.013.

Reino, C., van Loosdrecht, M., Carrera, J., Pérez, J., 2017. Effect of temperature on N_2O emissions from a highly enriched nitrifying granular sludge performing partial nitrification of a low strength wastewater. Chemosphere 336–343. https://doi.org/10.1016/j.chemosphere.2017.07.017.

Soreanu, G., Seto, P., Béland, M., Edmonson, K., Falletta, P., 2008. Investigation on the use of nitrified wastewater for the steady-state operation of a biotrickling filter for the removal of hydrogen sulphide in biogas. J. Environ. Eng. Sci. 7, 543–552. https://doi.org/10.1139/S08-023.

Svehla, P., Radechovska, H., Pacek, L., Michal, P., Hanc, A., Tlustos, P., 2017. Nitrification in a completely stirred tank reactor treating the liquid phase of digestate: the way towards rational use of nitrogen. Waste Manag. 64, 96–106. https://doi.org/10.1016/j.wasman.2017.03.041.

Tanikawa, D., Fujise, R., Kondo, Y., Fujihira, T., Seo, S., 2018. Elimination of hydrogen sulfide from biogas by a two-stage trickling filter system using effluent from anaerobic-aerobic wastewater treatment. Int. Biodeterior. Biodegrad. 130, 98–101. https://doi.org/10.1016/j.ibiod.2018.04.007.

Tomàs, M., Fortuny, M., Lao, C., Gabriel, D., Lafuente, Javier, Gamisans, X., 2009. Technical and economical study of a full-scale biotrickling filter for H_2S removal from biogas. Water Pract. Technol. 26–33. https://doi.org/10.2166/wpt.2009.026.

Wang, H., Feng, C., Deng, Y., 2020. Effect of potassium on nitrate removal from groundwater in agricultural waste-based heterotrophic denitrification system. Sci. Total Environ. 703, 134830. https://doi.org/10.1016/j.scitotenv.2019.134830.

Wang, J., Lu, H., Chen, G.-H., Lau, G.N., Tsang, W.L., van Loosdrecht, M.C.M., 2009. A novel sulfate reduction, autotrophic denitrification, nitrification integrated (SANI) process for saline wastewater treatment. Water Res. 43, 2363–2372. https://doi.org/10.1016/j.watres.2009.02.03.

Watsuntorn, W., Khanongnuch, R., Chulalaksananukul, W., Rene, E.R., Lens, P.N.L., 2020. Resilient performance of an anoxic biotrickling filter for hydrogen sulphide removal from a biogas mimic: steady, transient state and neural network evaluation.

J. Clean. Prod. 249, 119351. https://doi.org/10.1016/j.jclepro.2019.119351 evaluation. J. Clean. Prod. 249, 119351.
Xu, X.J., Li, H.J., Wang, W., Zhang, R.-C., Zhou, X., Xing, D.F., Ren, N.Q., Lee, D.J., Yuan, Y.X., Liu, L.H., Chen, C., 2020. The performance of simultaneous denitrification and biogas desulfurization system for the treatment of domestic sewage. Chem. Eng. J. 399, 125855. https://doi.org/10.1016/j.cej.2020.125855.
Zeng, Y., Luo, Y., Huan, C., Shuai, Y., Liu, Y., Xu, L., Ji, G., Yan, Z., 2019. Anoxic biodesulfurization using biogas digestion slurry in biotrickling filters. J. Clean. Prod. 224, 88–99. https://doi.org/10.1016/J.JCLEPRO.2019.03.218.